RSC Advances

PAPER

View Article Online
View Journal | View Issue

Cite this: *RSC Adv.*, 2020, **10**, 20579

Synergistic lubrication of a porous MoS_2-POSS nanohybrid†

Xiaoxuan Xu,[a] Songlong Jiao,[b] Zhengquan Liu[b] and Lei Liu *[b]

A porous MoS_2-polyhedral oligomeric silsesquioxane (POSS) nanohybrid was prepared from octavinyl-POSS nanoparticles and MoS_2 nanosheets for the first time, the structure and composition of which were confirmed by X-ray powder diffraction (XRD), Fourier-transform infrared spectra (FTIR), scanning electron microscopy (SEM), energy dispersive spectra (EDS) and thermal gravimetric analysis (TGA). As a comparison, MoS_2 nanosheets, octavinyl-POSS and MoS_2-POSS nanohybrid were used as lubricating additives for liquid paraffin (LP), which decreased the friction coefficients of LP by 7.8% (MoS_2), 14.1% (octavinyl-POSS), and 18.8% (MoS_2-POSS). Compared with MoS_2 and octavinyl-POSS, the MoS_2-POSS nanohybrid can be dispersed in organic solvents more homogeneously without adscititious dispersants or surfactants due to its better organic compatibilities. SEM and EDS analyses indicate that a synergistic frictional effect is responsible for the improved friction-reduction and anti-wear behavior.

Received 3rd March 2020
Accepted 11th May 2020

DOI: 10.1039/d0ra02014a

rsc.li/rsc-advances

1. Introduction

Molybdenum disulfide (MoS_2) occurs naturally as a lamellar hexagonal architecture composed of three stacked atomic layers (S–Mo–S) held together by weak van der Waals interactions.[1–3] MoS_2 with a definite 2D nanostructure shows promise for applications such as sensing,[4,5] catalysis,[6,7] and battery electrodes.[8,9] Moreover, MoS_2 is also an excellent lubricant additive due to its interlayer sliding properties.[10,11] MoS_2 with different morphologies, such as flower-like,[12] coral-like,[13] sphere-like,[14] or sheet-like[15] structures, has been prepared by hydrothermal methods, and these forms can used as lubricant additives to improve tribological properties.[16–18] Meanwhile, achieving better lubricating behavior for MoS_2 is a challenge because of its poor dispersion stability in liquid systems.[19]

On the other hand, reports have shown that polyhedral oligomeric silsesquioxanes (POSS) with a cube-octameric framework can also be utilized as lubricant additives to improve the properties of liquid lubricating systems. For example, Luca introduced POSS-NH_2 groups onto GO nanosheets, which reduced the friction coefficient;[20] Bhushan found that low amounts (0.5 wt% to 3.0 wt%) of POSS ingredients improved the friction and wear resistance of polymers and polymer composites.[21] As a kind of organic–inorganic nanoparticle, POSS has eight organic groups (R) surrounding an inorganic cubic Si–O–Si cage-shaped structure, where "R" stands for hydrogen or any alkyl, alkylene, aryl, or arylene group, or organic-functional derivatives of them.[22–25] The presence of organic groups makes it soluble in many organic solvents. More importantly, the organic groups can be used as functionalized sites and further expand its applications.[26,27]

MoS_2 nanosheets and POSS nanoparticles are common additives for lubricants because of their special characteristics and excellent performance. To our knowledge, the preparation and tribological properties of porous MoS_2-POSS nanohybrids have not been reported. In this work, in order to combine the individual advantages of MoS_2 and POSS, a novel kind of additive for a lubricating system named MoS_2-POSS is developed. A specific POSS molecule can be used as a potential modifier to achieve MoS_2 hybrid materials with improved tribological properties. Obviously, modification can provide MoS_2 with better dispersibility in the organic phase; on the other hand, the cooperation of POSS partly changes the lubrication mechanism. The friction–reduction properties of LP were measured using a pin-on-disk wear tester, and the related synergistic lubricating mechanism was investigated systematically.

2. Experimental

2.1. Materials

$(NH_4)_6Mo_7O_{24}\cdot 4H_2O$ and CN_2H_4S were provided by Sinopharm Chemical Reagent Co., Ltd. *n*-Butyl lithium (2.5 M in hexane) was acquired from Alfa Aesar without further purification. Octavinyl-POSS was purchased from Hybrid-Plastics™. Dithioglycol (DITG) was obtained from Aladdin Industrial Corporation (Shanghai, China). Azobisisobutyronitrile (AIBN) was provided by Shanghai National Medicine Group Chemical Reagent Co.,

[a]School of business and Trade, Nanjing Institute of Industry Technology, Nanjing 210023, People's Republic of China

[b]School of Mechanical Engineering, Southeast University, Nanjing 211189, People's Republic of China. E-mail: liulei@seu.edu.cn

† Electronic supplementary information (ESI) available. See DOI: 10.1039/d0ra02014a

Ltd. Tetrahydrofuran (THF) and *n*-hexane were commercially available and of analytical grade.

2.2. Preparation of the MoS_2-POSS nanohybrid

2.2.1 Bulk MoS_2. $(NH_4)_6Mo_7O_{24}\cdot 4H_2O$ (0.11 g) and CN_2H_4S (2.50 g) were dispersed in deionized water (52 mL) by ultrasonic treatment (20 min) to form a uniform mixture. The solution was decanted to a 100 mL Teflon-lined stainless steel autoclave and kept at 180 °C for 12 h. After the reaction, the acquired product was washed with deionized water and absolute ethyl alcohol several times and then dried at 80 °C.[28]

2.2.2 Preparation of Li_xMoS_2. A certain amount of bulk MoS_2 powder was added into 30 mL of an *n*-hexane solution of *n*-butyl lithium (0.50 M), and the mixture was transferred into a Teflon-lined stainless-steel autoclave. Subsequently, the sealed autoclave was heated to 220 °C and maintained at this temperature for 24 h. After cooling to room temperature, the mixture was rinsed with anhydrous hexane several times. The obtained solid (denoted Li_xMoS_2) was dried in a vacuum at 60 °C for 12 h.[29]

2.2.3 Preparation of DITG-MoS_2. 0.15 g of Li_xMoS_2 was dissolved in 150 mL of deionized water, followed by 4 h of ultrasonication. Finally, the suspension was neutralized using dilute nitric acid. The obtained suspension (few-layered MoS_2) and an excess amount of dithioglycol (DITG) were added into tetrahydrofuran (THF). After 8 h of stirring, the solution was centrifuged and washed with THF several times, and the collected precipitate (denoted DITG-MoS_2) was dried in a vacuum at 60 °C for 12 h.

2.2.4 Preparation of the MoS_2-POSS nanohybrid.[30] The received DITG-MoS_2 was added into a 250 mL three-necked round-bottom flask containing 60 mL of dry THF, and 0.15 g of octavinyl-POSS was added. Then, the solution mixture was magnetically stirred and refluxed for 30 minutes under a nitrogen atmosphere. Additionally, 6.7 mg of AIBN was added successively and the solution was purged with nitrogen for another 15 minutes. Then, the reaction system was held at 80 °C for 6 h. After the reaction product was filtered and dried under a vacuum at 60 °C for 4 h, the target MoS_2-POSS nanohybrid was obtained.

2.3. Techniques

FTIR spectra were recorded on a MAGNA-IR 750 spectrometer. XRD patterns were collected using a Rigaku K/max-γA X-ray diffractometer with Cu-Kα radiation (λ = 1.5415 Å) at a scanning rate of 0.02° s^{-1}. A Netzsch STA-409c Thermal Analyzer was used for TGA under a 50 × 10^3 mm^3 min^{-1} nitrogen flow with a heating rate of 10 °C min^{-1}; SEM and EDS characterization of the worn ball surface were carried out on an FEI Inspect F50 instrument.

2.4. Tribological tests

The tribological properties of the liquid paraffin (LP) mixtures were evaluated on an MW-W1A vertical universal friction and wear tester (Jinan, China) using a pin-on-disk sliding pair. It worked at a rotating speed of 200 rpm under a constant load of 250 N for a testing duration of 30 minutes; the friction pins used in this study were made of 45 steel (diameter: 4.8 mm; hardness: 44–46 HRC; surface roughness: 0.0125 μm). An Al_2O_3 disk (diameter: 42 mm; thickness: 5 mm; surface roughness: 0.0125 μm) was made by Suzhou Crystal Element Company in China.

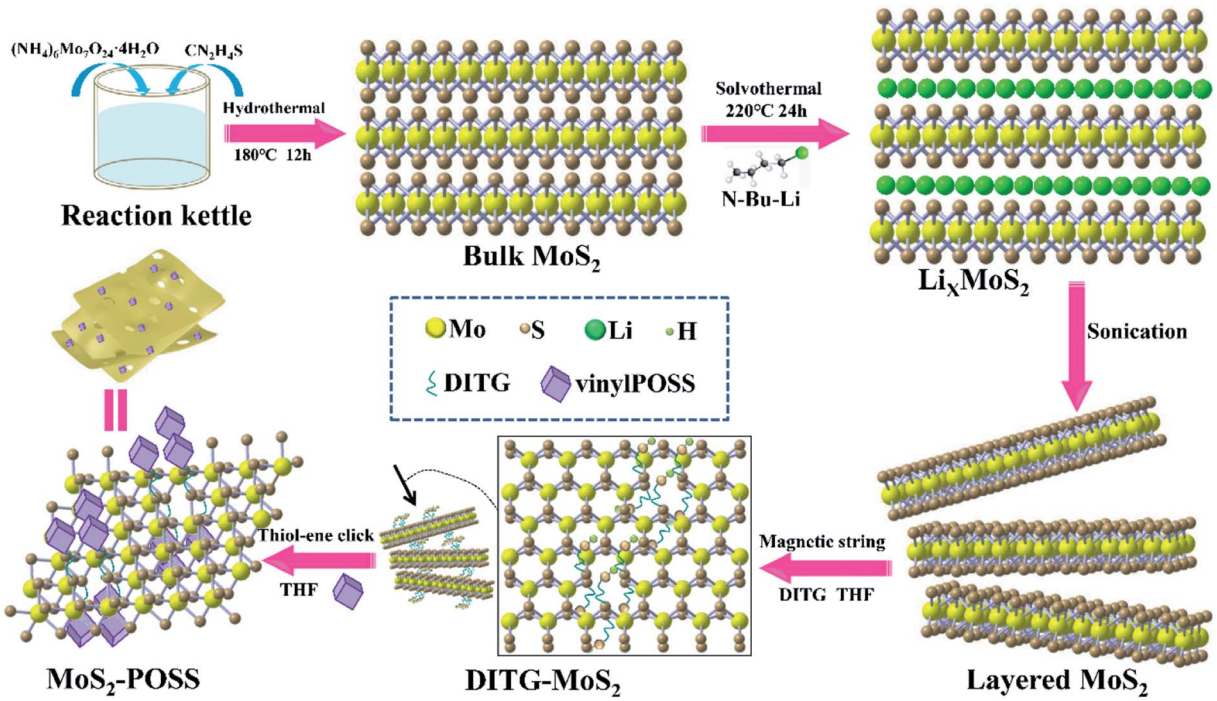

Fig. 1 Schematic representation of the synthesis of the MoS_2-POSS nanohybrid.

Friction and wear tests were performed at least three times under the same conditions so as to minimize data scattering, and the final friction data was obtained by calculating an average value of FC for different times.

3. Results and discussion

3.1 Characterization

The MoS_2-POSS nanohybrid was prepared as shown schematically in Fig. 1. Li_xMoS_2 was prepared using a solvothermal method. The *n*-hexane solution of *n*-butyl lithium is a mild and effective reagent for the insertion of Li into MoS_2. The reaction equation is as follows.[29]

$$MoS_2 + n\text{-Bu-Li} \rightarrow [MoS^{2-} + Bu^{-} + Li^{+}] \rightarrow LiMoS_2 + n\text{-}C_8H_{18}$$

DITH can act as a metal complexing agent that combines with a variety of metal ions to form stable complexes.[31] Dithioglycol (DITG) works as a "bridge" to connect MoS_2 nanosheets and POSS (Fig. S1†). Since the exfoliated MOS_2 nanosheets have extensive sulfur vacancy defects, DITG as a thiol can fill the vacancies to form Mo–S bonds.[32] Moreover, DITG can undergo a thiol-ene click reaction with the alkenyl group on POSS.[33] Therefore, MoS_2 and POSS can be tightly connected *via* DITG. With the introduction of DITG and POSS, POSS and DITG form a network polymer chain. The fragmented MoS_2 nanosheets will be actively and randomly adsorbed on the polymer chain, forming a loose and porous structure (Fig. S2†).

From Fig. 2a, it can be seen that the prepared MoS_2 is a random stack of many nanosheets. As shown in Fig. S2a,† the bulk MoS_2 obtained *via* the hydrothermal reaction shows obvious agglomeration, and shows multiple layers and a large size. Fig. S2b† shows that the exfoliated MoS_2 nanosheets are fragmented and thin. Selected area electron diffraction (SAED) shows that the obtained exfoliated MoS_2 nanosheets have a symmetrical and hexagonal structure, indicating that the Li^+ ultrasonic intercalation did not destroy the original nanostructure of MoS_2. The MoS_2-POSS nanohybrid has a loose and porous structure, and many holes can be observed on its surface (Fig. 2b). As shown in Fig. 2c–h, there is a uniform distribution of Si, O, S, and Mo elements throughout the MoS_2-POSS nanohybrid. The existence of the Si element proves that POSS has been successfully loaded onto the MoS_2 nanosheets. The content of the S and Mo elements indicates that MoS_2 dominates in the nanohybrid.

Fig. 3a gives the XRD patterns for MoS_2, Li_xMoS_2 and MoS_2-POSS. The curve of MoS_2 has an intense reflection at $2\theta = 14.46^\circ$, which corresponds to the 2H MoS_2 structure (0.61 nm).[34] After Li-ion intercalation, all of the diffractive peaks shift

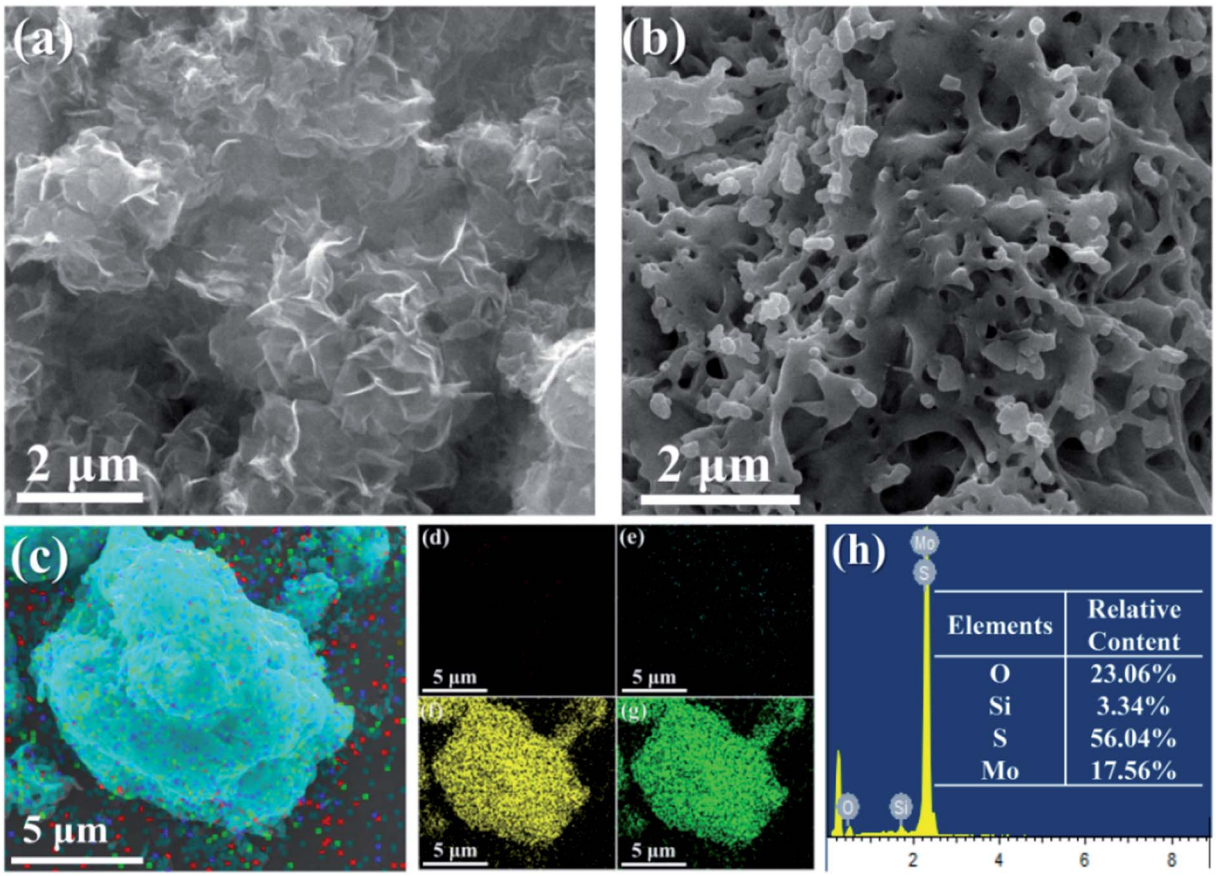

Fig. 2 SEM images of (a) MoS_2 and (b) the MoS_2-POSS nanohybrid. EDS mapping analysis of (c) MoS_2-POSS nanohybrid, element mapping analysis of (d) Si, (e) O, (f) S, (g) Mo, respectively; EDS spectra of MoS_2-POSS nanohybrid (h).

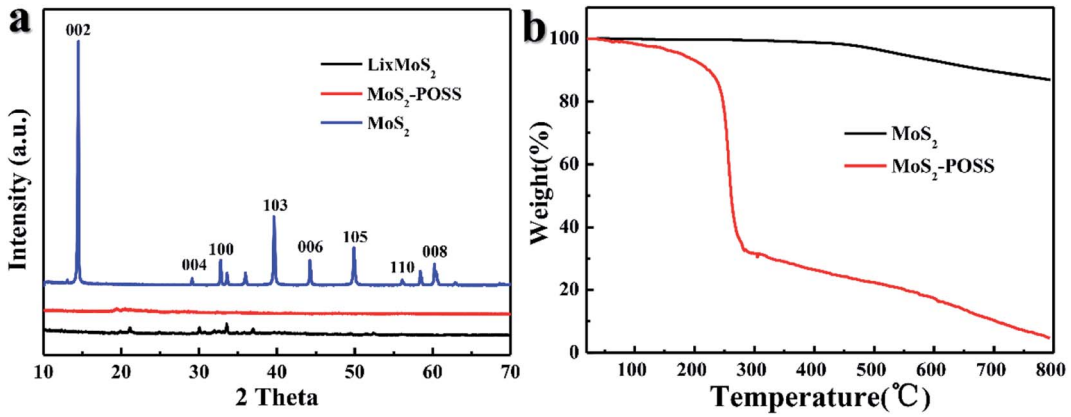

Fig. 3 (a) XRD patterns of MoS_2, Li_xMoS_2, and MoS_2-POSS nanohybrid, (b) thermal gravimetric analysis (TGA) curves of MoS_2, MoS_2-POSS with a heating rate of 10 °C min^{-1} under a nitrogen atmosphere.

to a lower-angle direction, which indicates that the intercalation increases the interlayer spacing of MoS_2.[35] Compared with the curves for unmodified MoS_2 and Li_xMoS_2, no obvious peaks can be detected for the MoS_2-POSS nanohybrid, which suggests their amorphous structure. On the other hand, TGA curves in Fig. 3b show that the major weight loss for MoS_2 emerges from about 500 °C, which can be attributed to its thermal decomposition. The MoS_2-POSS nanohybrid shows a different weight loss: a mass loss of 65% over the range of 200 to 290 °C due to the degradation of octavinyl-POSS and alkyl mercaptan; a slow and steady mass loss of POSS-MoS_2 after 300 °C is attributed to the decomposition of other organic phases and MoS_2.

FTIR spectra of MoS_2 nanosheets and the MoS_2-POSS nanohybrid are presented in Fig. 4a. The absorption peaks at 1180 and 1105 cm^{-1} are ascribed to the characteristic stretching of the Si–O–Si band in POSS. Moreover, the peaks at 2911 and 2848 cm^{-1} correspond to the $-CH_3$ and $=CH_2$ groups in the nanohybrid.[35] Good dispersity is the key to ensuring a stable friction performance for a lubricant. As shown in Fig. 4b, LP containing MoS_2 was black initially, but MoS_2 precipitated to the bottom and the solutions turned clear after 2 days. The color of MoS_2-POSS showed almost no change after 2 days, indicating that MoS_2-POSS has better dispersity than MoS_2 in LP. Octavinyl-POSS has eight functional groups, which can react with DITG or other organics, giving MoS_2-POSS better organic compatibility in liquid paraffin.

3.2 Tribological properties

Fig. 5 shows the changing trend of the friction coefficient with additive concentration. At first, the friction coefficient gradually decreases with an increase in MoS_2 or octavinyl-POSS concentration, and it increases when the additive concentration continues to increase beyond a certain value. Based on our results, the optimal concentration of octavinyl-POSS in LP is 0.60 wt%, and the corresponding value of the friction coefficient is 0.110, which is reduced by 14.1% compared with pure LP (friction coefficient: 0.128). Similarly, the optimal concentration

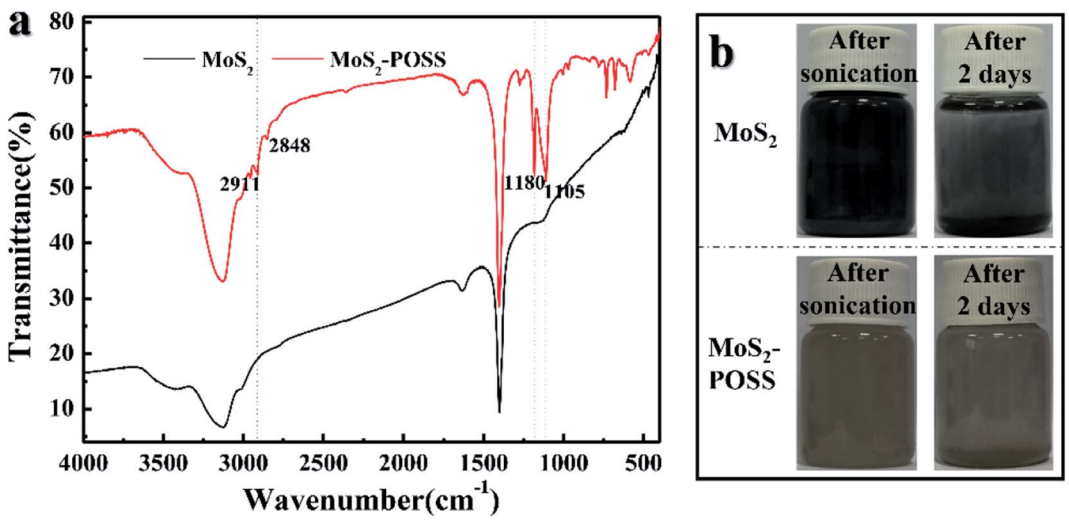

Fig. 4 (a) FTIR spectra of MoS_2 and MoS_2-POSS; (b) photographs before and after 2 days of dispersion for the LP containing MoS_2 and MoS_2-POSS with a content of 0.5 wt%.

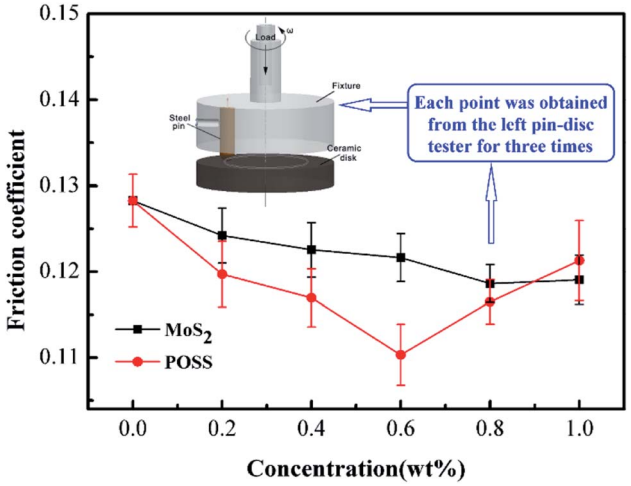

Fig. 5 Friction coefficient with different concentrations of MoS_2 and POSS.

for pure MoS_2 is 0.80 wt% and the corresponding value of the minimum friction coefficient is 0.118.

Meanwhile, Fig. 6 gives the real-time variation in the friction coefficient under lubrication by LP mixtures with different concentrations of MoS_2-POSS nanohybrid. The real-time friction coefficient of each system starts from a similar value at first, and all of the fiction coefficients increase gradually except for that of an LP mixture containing 0.40 wt% of MoS_2-POSS nanohybrid. The average friction coefficient curve displays a typical concave shape and thus the lowest friction coefficient is achieved by using an LP mixture containing 0.40 wt% of MoS_2-POSS nanohybrid, which gives a reduction of 18.8% when compared with that lubricated by pure LP. A certain concentration of MoS_2-POSS nanohybrid is advantageous for

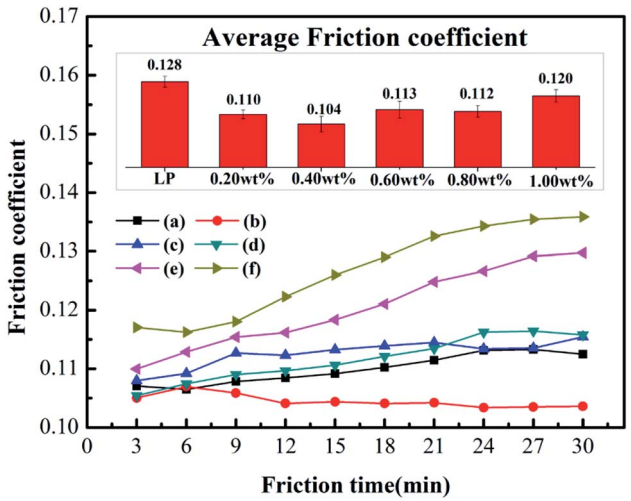

Fig. 6 Real-time changing trend of friction coefficient over time obtained from LP mixtures containing different MoS_2-POSS concentrations. (a) 0.20 wt%; (b) 0.40 wt%; (c) 0.60 wt%; (d) 0.80 wt%; (e) 1.00 wt%; (f) pure LP. The inserted picture is the average friction coefficient for (a)–(f).

improving the frictional performance of LP, but too higher concentration will result in a decrease of in wear resistance and an increase in the friction coefficient.

3.3 Synergistic lubrication

LP with an MoS_2-POSS nanohybrid possesses better friction-reduction and anti-wear properties than pure MoS_2 or POSS, which is attributed to the synergistic effect of MoS_2 and octavinyl-POSS. MoS_2 possesses excellent load-carrying capacity and low shear strength, but has poor organic compatibilities. Octavinyl-POSS possesses good organic solubility and self-lubricating properties. The introduction of octavinyl-POSS into MoS_2 nanosheets allows the nanohybrid to disperse in organic solvents more homogeneously. It can enter the contact areas of the frictional surfaces, thereby forming a protective and lubricious film to reduce the friction coefficient.

The morphologies of the worn surfaces after friction tests lubricated by LP with MoS_2 (Fig. 7) and POSS (Fig. S4†) give supplementary evidence for the trend in the change in friction coefficient. As shown in Fig. 7a, there are many deep pits and large areas of delamination on the worn surface, suggesting extremely adhesive wear and no continuous tribo-film under the lubrication of LP containing 0.20 wt% of MoS_2. While the worn surfaces lubricated with higher concentrations of MoS_2 show obvious hints of mild scuffing structures, indicating that more MoS_2 has participated in the friction process, leading to the formation of a compact and intact tribo-film. The tribo-films can prevent direct metal friction and abrasion wear. In Fig. S4a,† a large number of deep pits and furrows can be found on the worn surface for the case of using LP containing 0.20 wt% of octavinyl-POSS. The worn surface shows small pits and shallow furrows when the content reaches 0.60 wt%, corresponding to the lowest friction coefficient. With the concentration increasing, the rough wear scar in association with severe scuffing can be found again in Fig. S4D and S4E.† These results agree with the trend in the change in the friction coefficient.

Fig. 8 shows the morphologies of steel pins lubricated by pure LP and LP containing MoS_2-POSS nanohybrid. Under pure LP lubrication, severely worn surfaces can be observed and a large area is spalled by a strong shear force. Unlike the above results, the worn surfaces lubricated by LP with MoS_2-POSS nanohybrid are smoother and the related furrows are shallower or narrower. The best lubrication can be achieved when the MoS_2-POSS concentration is 0.40 wt%, and the worn surface becomes smoother when it is coated by a protective layer. Therefore, the MoS_2-POSS nanohybrid exhibits synergistic lubrication and anti-wear properties compared to pure MoS_2 or POSS.

Micro-area elemental analysis of the worn surface is an effective way to understand the friction-reducing mechanism. As shown in Fig. S5(a-1, a-2 and a-3†), Si element is observed on the worn surfaces lubricated by LP containing POSS. This indicates that adsorbed tribo-layers made up of POSS or Si containing materials have formed on the worn surfaces, which can prevent direct contact between asperities and reduce the

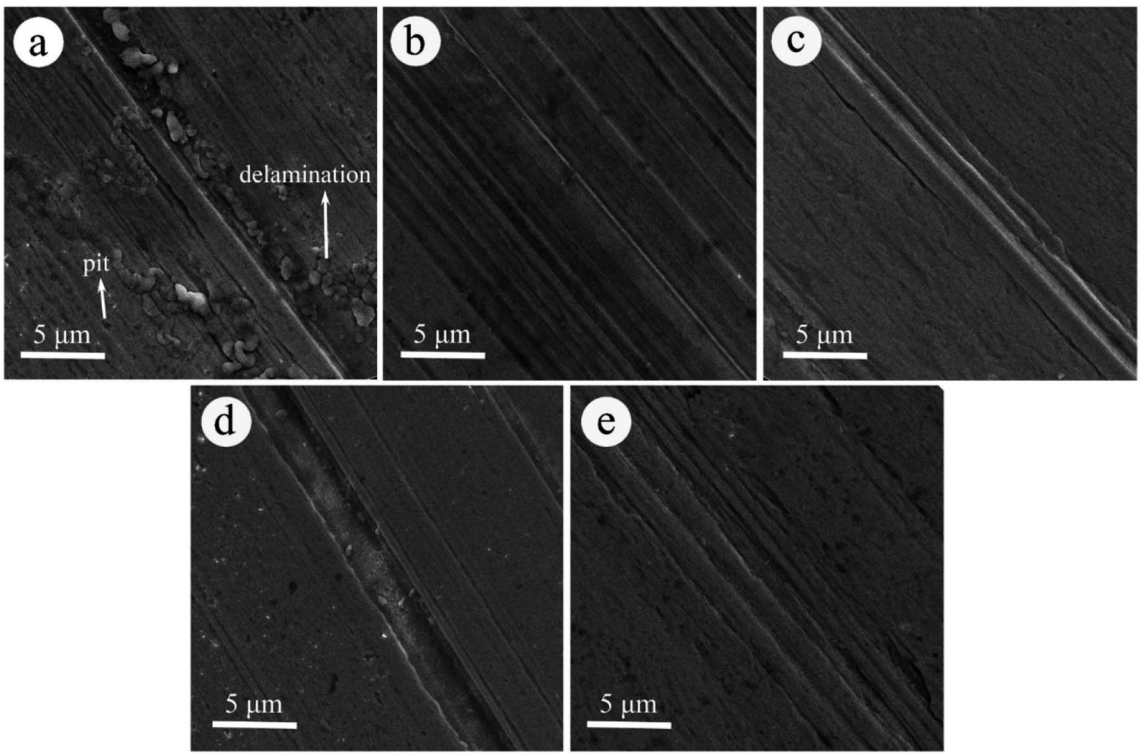

Fig. 7 SEM images of the worn surface on pins lubricated with LP containing: (a) 0.20 wt%, (b) 0.40 wt%, (c) 0.60 wt%, (d) 0.80 wt%, and (e) 1.00 wt% of MoS_2.

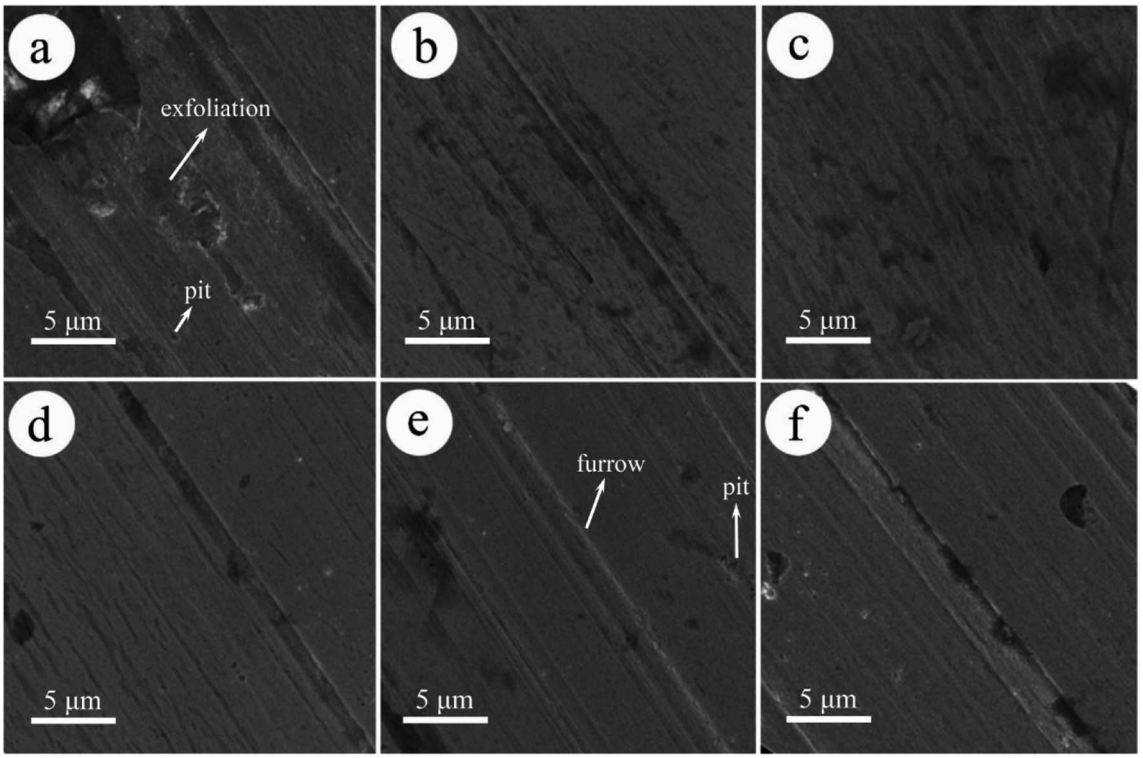

Fig. 8 SEM images of the worn surface on pins lubricated with (a) LP and LP containing: (b) 0.20 wt%, (c) 0.40 wt%, (d) 0.60 wt%, (e) 0.80 wt%, and (f) 1.00 wt% MoS_2-POSS.

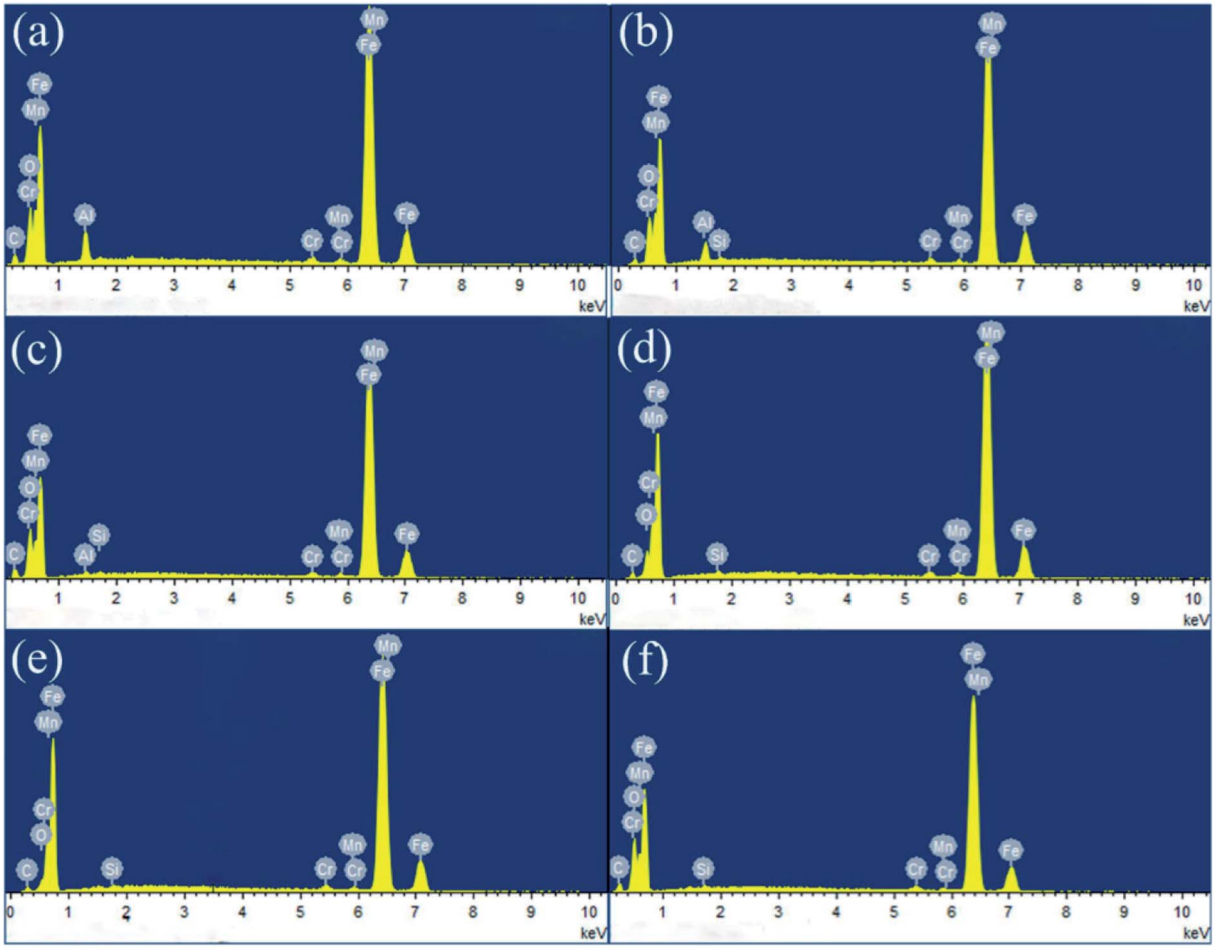

Fig. 9 EDS spectra of wear scars for steel pins lubricated by (a) LP and LP containing (b) 0.20 wt%, (c) 0.40 wt%, (d) 0.60 wt%, (e) 0.80 wt%, and (f) 1.00 wt% MoS_2-POSS, respectively.

friction and wear. On the other hand, Mo or S elements are not found on the frictional surfaces lubricated by LP containing MoS_2, as shown in Fig. S5(b-1, b-2 and b-3†). Considering the poor deposition ability on the contact areas, it can be inferred that the layered MoS_2 plays only an intermediary role during the sliding process. In the initial stage, MoS_2 can enter and stay in the contact area of the worn surfaces. With an increase in friction time, the layered structure will be pushed out of the friction pairs. In addition, Al element is not found on the surfaces in Fig. S5,† which may be attributed to a "separation effect" caused by layered MoS_2 and octavinyl-POSS.

EDS analysis of the worn surfaces lubricated by LP containing MoS_2-POSS nanohybrid (Fig. 9) shows that Si element exists on the worn surface, which suggests that a tribo-film has formed between the surfaces of the friction pairs. It is quite interesting that the Al element is decreased in a regular trend (Table 1), which is due to the fact that more additives enter the frictional areas and prevent the direct contact of frictional surfaces. The changing trend with amount of MoS_2-POSS is similar to that of the friction coefficient, showing that a much higher concentration of additive is disadvantageous to a further improvement in friction performance. A higher concentration of nanohybrid may prevent the friction pairs from making direct contact, and excessive nanohybrid in LP will result in random aggregation on the surface of the friction pairs.

Table 1 Weight fraction of Al on steel pins lubricated by LP containing different concentrations of MoS_2-POSS

Element	LP	0.20%	0.40%	0.60%	0.80%	1.00%
Al	3.6	2.63	0.37	0	0	0

Octavinyl-POSS with a rather small size and large surface area can easily fill up the micro-scratches or nano-gaps in the surfaces, consequently leading to lower friction and wear (Fig. 10a). When the two frictional surfaces are in contact with each other, relative slip occurs between the MoS_2 layers (Fig. 10b). MoS_2 nanosheets will form fragments to fill the pits due to the pressure and shear force, which can effectively improve the anti-wear ability and load-carrying capacity of LP. However, inorganic MoS_2 is hardly adsorbed on the frictional surfaces and can be easily pushed out of the friction pairs at last. An MoS_2-POSS nanohybrid combines the advantages of MoS_2 and POSS, giving a lower friction coefficient and

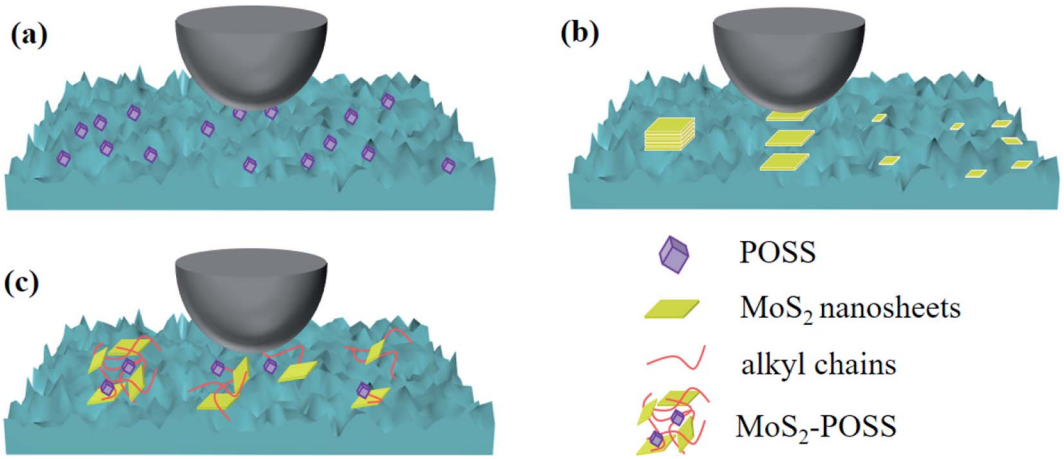

Fig. 10 Schematics of the lubrication mechanism of (a) octavinyl-POSS nanoparticle, (b) MoS_2 nanosheet and (c) MoS_2-POSS nanohybrid.

a smoother friction surface (Fig. 10c). On the one hand, octavinyl-POSS is an excellent coating deposited on the metal surface for low friction and can improve the dispersity of an MoS_2-POSS nanohybrid in LP. On the other hand, MoS_2 possesses excellent anti-wear and extreme-pressure properties. The porous structure of the nanohybrid has excellent adsorption properties for lubricating oil, which can increase the thickness of the lubricating film on the friction surface. The synergistic effect can improve the friction–reduction and anti-wear properties of pure LP remarkably, making an MoS_2-POSS nanohybrid into an excellent lubricant additive.

4. Conclusions

In summary, a porous MoS_2-POSS nanohybrid has been synthesized *via* a hydrothermal method for the first time, and it is highly soluble in the organic phase without extra surfactants or dispersants. As an additive, it can improve the tribological properties of LP effectively, and give the mixtures better friction-reduction and anti-wear abilities compared with pure MoS_2 or POSS. Based on experimental results, some fundamental understanding of the synergistic lubrication mechanism generated by MoS_2 and POSS has been suggested, which can provide some scientific value and promising application prospects.

Conflicts of interest

There are no conflicts to declare.

Acknowledgements

This work is financially supported by the Natural Science Foundation of China (51805248).

References

1 J. N. Coleman, M. Lotya, A. O'Neill, S. D. Bergin, P. J. King, U. Khan and I. V. Shvets, Two-dimensional nanosheets produced by liquid exfoliation of layered materials, *Science*, 2011, **331**, 568–571.
2 M. Chhowalla, H. S. Shin, G. Eda, L. J. Li, K. P. Loh and H. Zhang, The chemistry of two-dimensional layered transition metal dichalcogenide nanosheets, *Nat. Chem.*, 2013, **5**, 263–275.
3 V. Nicolosi, M. Chhowalla, M. G. Kanatzidis and M. S. Strano, Liquid exfoliation of layered materials, *Science*, 2013, **340**, 1420–1438.
4 H. Li, Z. Yin, Q. He, H. Li, X. Huang, G. Lu and H. Zhang, Fabrication of single-and multilayer MoS_2 film-based field-effect transistors for sensing NO at room temperature, *Small*, 2012, **8**, 63–67.
5 F. K. Perkins, A. L. Friedman, E. Cobas, P. M. Campbell, G. G. Jernigan and B. T. Jonker, Chemical vapor sensing with monolayer MoS_2, *Nano Lett.*, 2013, **13**, 668–673.
6 N. Tian, Z. Li, D. Xu, Y. Li, W. Peng, G. Zhang and X. Fan, Utilization of MoS_2 nanosheets to enhance the photocatalytic activity of ZnO for the aerobic oxidation of benzyl halides under visible light, *Ind. Eng. Chem. Res.*, 2016, **55**, 8726–8732.
7 Y. Sun, F. Alimohammadi, D. Zhang and G. Guo, Enabling colloidal synthesis of edge-oriented MoS_2 with expanded interlayer spacing for enhanced HER catalysis, *Nano Lett.*, 2017, **17**, 1963–1969.
8 J. Xiao, D. Choi, L. Cosimbescu, P. Koech, J. Liu and J. P. Lemmon, Exfoliated MoS_2 nanocomposite as an anode material for lithium ion batteries, *Chem. Mater.*, 2010, **22**, 4522–4524.
9 X. Xie, T. Makaryan, M. Zhao, K. L. Van Aken, Y. Gogotsi and G. Wang, MoS_2 Nanosheets Vertically Aligned on Carbon Paper: A Freestanding Electrode for Highly Reversible Sodium-Ion Batteries, *Adv. Energy Mater.*, 2016, **6**, 1502161–1502167.
10 M. Kalin, J. Kogovšek and M. Remškar, Mechanisms and improvements in the friction and wear behavior using MoS_2 nanotubes as potential oil additives, *Wear*, 2012, **280**, 36–45.

11 S. P. Vattikuti, C. Byon, C. V. Reddy, B. Venkatesh and J. Shim, Synthesis and structural characterization of MoS_2 nanospheres and nanosheets using solvothermal method, *J. Mater. Sci.*, 2015, **50**, 5024–5038.

12 G. Tang, J. Zhang, C. Liu, D. Zhang, Y. Wang, H. Tang and C. Li, Synthesis and tribological properties of flower-like MoS_2 microspheres, *Ceram. Int.*, 2014, **40**, 11575–11580.

13 L. Liu, Z. Huang and P. Huang, Fabrication of coral-like MoS_2 and its application in improving the tribological performance of liquid paraffin, *Tribol. Int.*, 2016, **104**, 303–308.

14 Z. Hu, X. Zhou, X. Fu and H. Shi, Lubricating properties of Cyanex 302-modified MoS_2 microspheres in base oil 500SN, *Lubric. Sci.*, 2007, **19**, 71–79.

15 H. Wu, L. Qin, G. Dong, M. Hua, S. Yang and J. Zhang, An investigation on the lubrication mechanism of MoS_2 nano sheet in point contact: The manner of particle entering the contact area, *Tribol. Int.*, 2017, **107**, 48–55.

16 W. Song, J. Yan and H. Ji, Tribological Study of the SOCNTs@ MoS_2 composite as a lubricant additive: synergistic effect, *Ind. Eng. Chem. Res.*, 2018, **57**, 6878–6887.

17 X. Jia, J. Huang, Y. Li, J. Yang and H. Song, Monodisperse Cu nanoparticles @ MoS_2 nanosheets as a lubricant additive for improved tribological properties, *Appl. Surf. Sci.*, 2019, **494**, 430–439.

18 T. Luo, X. Chen, L. Wang, P. Wang, C. Li, H. Zeng and B. Cao, Green laser irradiation-stimulated fullerene-like MoS_2 nanospheres for tribological applications, *Tribol. Int.*, 2018, **122**, 119–124.

19 C. Altavilla, M. Sarno and P. Ciambelli, A novel wet chemistry approach for the synthesis of hybrid 2D free-floating single or multilayer nanosheets of MS_2@ oleylamine (M = Mo, W), *Chem. Mater.*, 2011, **23**, 3879–3885.

20 L. Valentini, S. B. Bon, O. Monticelli and J. M. Kenny, Deposition of amino-functionalized polyhedral oligomeric silsesquioxanes on graphene oxide sheets immobilized onto an amino-silane modified silicon surface, *J. Mater. Chem.*, 2012, **22**, 6213–6217.

21 B. Bhushan, M. Palacio and S. Schricker, Effect of polyhedral oligomeric silsesquioxane concentration on the friction and wear of dental polymers, *J. Vac. Sci. Technol., A*, 2010, **28**, 713–718.

22 S. Y. Gu, S. P. Jin and L. L. Liu, Polyurethane/polyhedral oligomeric silsesquioxane shape memory nanocomposites with low trigger temperature and quick response, *J. Polym. Res.*, 2015, **22**, 1–9.

23 C. Petit, K. Y. A. Lin and A. H. A. Park, Design and characterization of liquidlike POSS-based hybrid nanomaterials synthesized *via* ionic bonding and their interactions with CO_2, *Langmuir*, 2013, **29**, 12234–12242.

24 W. H. Liao, S. Y. Yang, S. T. Hsiao, Y. S. Wang, S. M. Li, C. C. M. Ma and S. J. Zeng, Effect of octa (aminophenyl) polyhedral oligomeric silsesquioxane functionalized graphene oxide on the mechanical and dielectric properties of polyimide composites, *ACS Appl. Mater. Interfaces*, 2014, **6**, 15802.

25 Y. Li, C. Luo, X. Li, K. Zhang, Y. Zhao, K. Zhu and X. Yuan, Submicron/nano-structured icephobic surfaces made from fluorinated polymethylsiloxane and octavinyl-POSS, *Appl. Surf. Sci.*, 2016, **360**, 113–120.

26 W. Yu, J. Fu, X. Dong, L. Chen and L. Shi, A graphene hybrid material functionalized with POSS: synthesis and applications in low-dielectric epoxy composites, *Compos. Sci. Technol.*, 2014, **92**, 112–119.

27 S. D. Jiang, G. Tang, Z. M. Bai, Y. Y. Wang, Y. Hu and L. Song, Facile fabrication of POSS-Modified MoS_2/PMMA nanocomposites with enhanced thermal, mechanical and optical limiting properties, *RSC Adv.*, 2013, **4**, 3253–3262.

28 L. Liu, S. L. Jiao, Y. T. Peng and W. Zhou, A green design for lubrication: multifunctional system containing Fe_3O_4@ MoS_2 nanohybrid, *ACS Sustain. Chem. Eng.*, 2018, **6**, 7372–7379.

29 F. Xiong, H. Wang, X. Liu, J. Sun, M. Brongersma, E. Pop and Y. Cui, Li intercalation in MoS_2: in situ observation of its dynamics and tuning optical and electrical properties, *Nano Lett.*, 2015, **15**, 6777–6784.

30 S. D. Jiang, G. Tang, Z. M. Bai, Y. Y. Wang, Y. Hu and L. Song, Surface functionalization of MoS_2 with POSS for enhancing thermal, flame-retardant and mechanical properties in PVA composites, *RSC Adv.*, 2014, **4**, 3253–3262.

31 P. Han and Y. Xia, Thiol-functionalized metal–organic framework for highly efficient removal of bromate from water, *J. Environ. Chem. Eng.*, 2018, **6**, 3384–3391.

32 Q. Li, Y. H. Zhao, C. Y. Ling, S. J. Yuan, Q. Chen and J. L. Wang, Towards a comprehensive understanding of the reaction mechanisms between defective MoS_2 and thiol molecules, *Angew. Chem., Int. Ed.*, 2017, **129**, 10637–10641.

33 A. C. Pauly and F. Lena, Incorporating amino acid sequences into the backbone chain of polymers through thiol-ene chemistry, *Polymer*, 2015, **72**, 378–381.

34 D. Dumcenco, D. Ovchinnikov, K. Marinov, P. Lazic, M. Gibertini and N. Marzari, Large-area epitaxial monolayer MoS_2, *ACS Nano*, 2015, **9**, 4611–4620.

35 K. Chang, X. Hai, H. Pang, H. B. Zhang, L. Shi, G. G. Liu, H. M. Liu, G. X. Zhao, M. Li and J. H. Ye, Targeted synthesis of 2H- and 1T-phase MoS_2 monolayers for catalytic hydrogen evolution, *Adv. Mater.*, 2016, **28**, 10033–10041.